Manganese(II) pyrimidine-4,6-dicarboxylates: synthetic, structural, magnetic and adsorption insights into the system

Journal:	*Inorganic Chemistry*
Manuscript ID:	ic-2008-002788.R1
Manuscript Type:	Article
Date Submitted by the Author:	07-Apr-2008
Complete List of Authors:	Castillo, Oscar; University of the Basque Country, Inorganic Chemistry

Manganese(II) pyrimidine-4,6-dicarboxylates: synthetic, structural, magnetic and adsorption insights into the system

Garikoitz Beobide[a,b], Wen-guo Wang[c], Oscar Castillo[a,], Antonio Luque[a], Pascual Román[a], Giulia Tagliabue[c,d], Simona Galli[d,*] and Jorge A. R. Navarro[c,*]*

[a]Departamento de Química Inorgánica, Facultad de Ciencia y Tecnología, Universidad del País Vasco, Apartado 644, E–48080 Bilbao, Spain

[b]Departamento de Procesos de Fabricación, Fundación Tekniker, Avda Otaola 20, E-20600 Eibar, Spain

[c]Departamento de Química Inorgánica, Universidad de Granada Av. Fuentenueva S/N, E–18071 Granada, Spain

[d]Dipartimento di Scienze Chimiche e Ambientali, Università dell'Insubria Via Valleggio 11, I-22100 Como, Italy

Authors to whom correspondence should be addressed. E-mail: oscar.castillo@ehu.es; simona.galli@uninsubria.it; jarn@ugr.es

Graphical Contents Entry

A number of manganese coordination polymers, possessing different local structure, supramolecular features and hydration levels, have been isolated: their interconversion paths and functional properties have been deeply characterized.

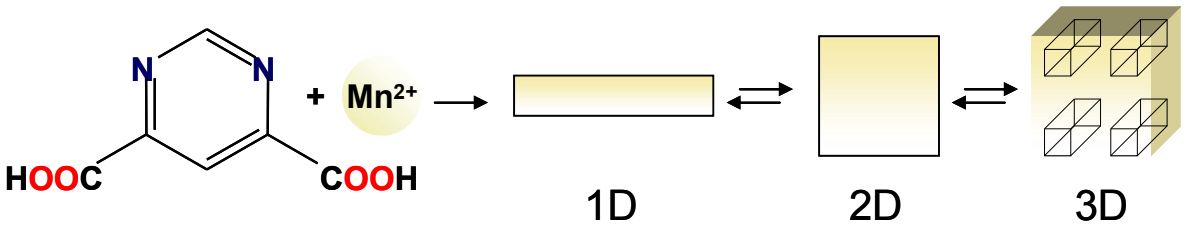

Abstract

A series of manganese(II) coordination polymers containing the pyrimidine–4,6–dicarboxylate (pmdc) bridging ligand has been prepared. The stoichiometry and structural features of these materials, ranging from 1D chains $\{[Mn(\mu\text{-pmdc})(H_2O)_3]\cdot 2H_2O\}_n$ (**1**), $\{[Mn_2(\mu\text{-pmdc})_2(H_2O)_5]\cdot 2H_2O\}_n$ (**2**) to 2D layers $\{[Mn(\mu_3\text{-pmdc})(H_2O)]\cdot H_2O\}_n$ (**3**) or to 3D porous networks $\{[Mn(pmdc)]\cdot 2H_2O\}_n$ (**4**), are extremely dependant on the synthetic conditions (*i.e.* temperature and solvent). In spite of the structural diversity of these systems, the crystallographic studies reveal that the pmdc ligand typically displays a tetradentate μ-(κO,κN:κO",κN') coordination mode (compounds **1**, **2** and **5**), with the carboxylate groups almost coplanar with the pyrimidine ring. In compound **3**, the pmdc moiety adopts a pentadentate μ_3-(κO,κN:κO",κN':κO) coordination type. The thermal, magnetic and adsorption properties of these systems have been studied. The results show that they behave as antiferromagnets, as a consequence of the efficient magnetic exchange through the pmdc bridges. **4** possesses permanent porosity, as proved by gas sorption (N_2 at 77 K and CO_2 at 293 K). Finally, a heteronuclear iron(II)/manganese(II) 1D chain $\{[FeMn(\mu\text{-pmdc})_2(H_2O)_5]\cdot 2H_2O\}_n$ (**5**), isomorphous to **2**, has also been prepared and fully characterized.

KEYWORDS. Pyrimidine–4,6–dicarboxylate, coordination polymers, porosity, adsorption, magnetic exchange, Heisenberg chain

Introduction

The study of the structural and functional properties of coordination networks and polymers is one of the fastest-growing areas in the chemical and material sciences, due to the wide variety of properties that they exhibit with a huge range of potential technological[1] and industrial[2] applications. The latter include high gas-storage capability of low density fuel gases at safe pressures and room temperature,[3] gas mixture separations,[4] selective heterogeneous catalysis,[5] with some examples of regio[6] and stereoselective processes,[7] and even controlled delivery of signal molecules (*e.g.* NO) for biological applications.[8] In addition, coordination networks have been prepared exhibiting bulk magnetism (hysteresis, spin-crossover, photomagnetism…), photophysical or electrical properties, second-harmonic generation.[1]

We have previously shown that the construction of extended coordination networks in a self-assembly process is facilitated by the use of simple and symmetric nitrogen heterocyclic ligands, which leads to the formation of materials possessing interesting functional aspects as non-linear optical,[9] magnetic,[10] thermal[11] and adsorption properties.[12,13] Worthy of note, the functionality of these systems can be finely tuned through the coupling of appropriate metal ions and ligands. In this regard, we have very recently reported a series of 1D coordination polymers of $\{[M(\mu\text{-pmdc})(H_2O)_2]\cdot H_2O\}_n$ formula (M = Fe, Co, Ni, Cu, Zn), obtained by a self-assembly process involving divalent first row transition metal ions and the symmetric pyrimidine-4,6-dicarboxylate (pmdc) species, typically acting in a tetradentate bischelate bridging mode.[14] In the present manuscript, we describe how the combination of this ligand with the coordination plasticity of the manganese(II) ion yielded, exploiting different synthetic conditions (Scheme 1), a variety of extended coordination compounds, ranging from 1D chains $\{[Mn(\mu\text{-pmdc})(H_2O)_3]\cdot 2H_2O\}_n$ (**1**); $\{[Mn_2(\mu\text{-pmdc})_2(H_2O)_5]\cdot 2H_2O\}_n$ (**2**), $\{[FeMn(\mu\text{-pmdc})_2(H_2O)_5]\cdot 2H_2O\}_n$ (**5**), to 2D layers $\{[Mn(\mu_3\text{-pmdc})(H_2O)]\cdot H_2O\}_n$ (**3**) and to 3D porous networks $\{[Mn(pmdc)]\cdot 2H_2O\}_n$ (**4**). These systems have been structurally characterised by single crystal and powder X-ray crystallographic methods and their thermal, magnetic and adsorption properties have been evaluated.

Insert SCHEME 1 near here

Experimental Section

Chemicals. All chemicals were of reagent grade and were used as commercially obtained. The starting material KHpmdc and H_2pmdc were prepared following the previously reported procedure.[15]

Synthesis of $\{[Mn(\mu\text{-pmdc})(H_2O)_3]\cdot 2H_2O\}_n$ (1). An aqueous solution (5 mL) of $Mn(NO_3)_2\cdot 4H_2O$ (0.0628 g, 0.25 mmol) was added dropwise to a solution (water 10 mL) of KHpmdc (0.0515 g, 0.25 mmol). The resulting light-yellow solution was allowed to evaporate at room temperature. Few days later colourless single-crystals of compound **1** were obtained. Yield: 80%. Compound **1**: Anal. Calcd for $C_6H_{12}MnN_2O_9$: C, 23.15; H, 3.89; N, 9.01; Mn, 17.66. Found: C, 23.20; H, 3.88; N, 9.10; Mn, 17.58. Main IR features (cm^{-1}, KBr pellet): 3464sh, 3367vs for ν(O–H); 3117w for ν(C–H); 1653vs for ν_{as}(O–C–O); 1600s for ν(C=C + C=N); 1471w for ν(C_{ar}–C); 1373vs for ν_s(O–C–O); 1311w, 1191w, 1093w for δ_{ip}(C–H); 1018w for δ_{op}(C–H); 928w for δ_{ring}; 729m for δ_{ip}(O–C–O); 698m for δ_{op}(O–C–O); 515w for τ_{ring}.

Synthesis of $\{[Mn_2(\mu\text{-pmdc})_2(H_2O)_5]\cdot 2H_2O\}_n$ (2) and $\{[Mn(\mu_3\text{-pmdc})(H_2O)]\cdot H_2O\}_n$ (3). Aqueous suspensions (15 mL) of compound **1** (0.0778 g, 0.25 mmol) were placed in a teflon vessel surrounded by a steel casing and placed on a heater. At temperatures above 50 ºC a mixture of crystals of compound **1** and **2** are obtained, whereas in the 70–75 ºC range only light pink crystals of compound **2** are obtained (yield: 70%). Finally, in the range 80–140 ºC yellow crystals of compound **3** are obtained (yield: 70%). Outside these temperature ranges a mixture of compounds is obtained. Compound **2**: Anal. Calcd for $C_{12}H_{18}MnN_4O_{15}$: C, 25.35; H, 3.19; N, 9.86; Mn, 19.35. Found: C, 25.26; H, 3.29; N, 9.91; Mn, 19.24. Main IR features (cm^{-1}, KBr pellet): 3460vs for ν(O–H); 3113w for ν(C–H); 1648vs for ν_{as}(O–C–O); 1597s, 1536s for ν(C=C + C=N); 1373vs for ν_s(O–C–O); 1188w, 1093w for δ_{ip}(C–H); 1021w for δ_{op}(C–H); 927w for δ_{ring}; 727m for δ_{ip}(O–C–O); 700m for δ_{op}(O–C–O); 515w for τ_{ring}; 415w for ν(M–O + M–N). Compound **3**: Anal. Calcd for $C_6H_6MnN_2O_6$: C, 28.02; H, 2.35; N, 10.90; Mn, 21.37. Found: C, 27.93; H, 2.24; N, 10.84; Mn, 21.37. Main IR features (cm^{-1}, KBr pellet): 3420vs for ν(O–H); 3120w for ν(C–H); 1671vs, 1636s for ν_{as}(O–C–O); 1604s, 1537m for ν(C=C + C=N); 1475w for ν(C_{ar}–C); 1364vs for ν_s(O–C–O);

1187w, 1107w for δ_{ip}(C–H); 1022w for δ_{op}(C–H); 924w for δ_{ring}; 742m for δ_{ip}(O–C–O); 693m for δ_{op}(O–C–O); 520w for τ_{ring}; 462w for ν(M–O + M–N).

Synthesis of $[Mn(pmdc)(H_2O)_3]_n$ (4). H_2pmdc (0.61 g, 3 mmol) was added to a solution of $Mn(ClO_4)_2{\cdot}6H_2O$(1.45 g, 4 mmol) in DMF (25 mL). The resulting suspension was heated with stirring at 110 ºC during 4 h giving rise to the formation of a yellow solid which was washed with DMF, ethanol and diethyl ether. Yield: 90%. Anal. Calcd for $C_6H_8MnN_2O_7$: C, 26.20; H, 2.93; N, 10.18; Mn, 19.97. Found: C, 26.37; H, 2.56; N, 10.21; Mn, 19.69. Main IR features (cm^{-1}, KBr pellet): 3425vs for ν(O–H); 1638vs for ν_{as}(O–C–O); 1594s, 1545s for ν(C=C + C=N); 1382vs for ν_s(O–C–O); 1193w, 1093w for δ_{ip}(C–H); 1025w for δ_{op}(C–H); 933w for δ_{ring}; 735m for δ_{ip}(O–C–O); 539w for τ_{ring}; 468w for ν(M–O + M–N).

Synthesis of $\{[FeMn(\mu\text{-}pmdc)_2(H_2O)_5]{\cdot}2H_2O\}_n$ (5). An aqueous solution (20 mL) containing H_2pmdc (2 mmol) and $Fe(ClO_4)_2{\cdot}6H_2O$ (0.25 g, 1 mmol) was heated at 90 ºC during 1 h giving rise to a dark solution. After cooling of the solution, solid $Mn(ClO_4)_2{\cdot}6H_2O$ (0.36 g, 1 mmol) was added giving rise to a dark red solution which after 1 month at room temperature yielded dark red crystals suitable for X-ray diffraction. Yield: 70%.Anal. Calcd for $C_{12}H_{18}FeMnN_4O_{15}$: C, 25.33; H, 3.19; N, 9.84; Mn, 9.65; Fe, 9.81. Found: C, 25.55; H, 3.19; N, 9.96; Mn, 9.63; Fe, 9.77. Main IR features (cm^{-1}, KBr pellet): 3406vs for ν(O–H); 1654vs for ν_{as}(O–C–O); 1599s, 1540s for ν(C=C + C=N); 1373vs for ν_s(O–C–O); 1189w for δ_{ip}(C–H); 1022w for δ_{op}(C–H); 927w for δ_{ring}; 728m for δ_{ip}(O–C–O); 696m for δ_{op}(O–C–O); 472w for ν(M–O + M–N).

Physical Measurements. Elemental analyses (C, H, N) were performed on a LECO CHNS–932 microanalytical analyzer. Metal content was determined by absorption spectrometry. The IR spectra (KBr pellets) were recorded on a FTIR Mattson 1000 spectrometer in the 4000–400 cm^{-1} spectral region. Thermal analysis (TG/DTG/DTA) were performed on a TA Instruments SDT 2960 thermal analyzer in a synthetic air atmosphere (79%N_2/21%O_2) with heating rate of 5 ºC min^{-1}. Magnetic measurements were performed on polycrystalline samples of the compounds with a Quantum Design

SQUID susceptometer covering the temperature range of 2.0–300 K at 0.5 T. The susceptibility data were corrected for the diamagnetism estimated from Pascal's tables,[16] the temperature-independent paramagnetism, and the magnetization of the sample holder. Sorption isotherms were measured on a Micromeritics Tristar 3000 volumetric instrument under continuous adsorption conditions. Prior to measurement, powder samples were heated at 130 °C for 2 h and outgassed to 10^{-3} Torr using a Micromeritics Flowprep. BET and Langmuir analyses have been used to determine the total specific surface area for the N_2 isotherms.

Single-Crystal X-ray Data Collection and Structure Determination. Data collections on single crystals of compounds **1–3** and **5** were carried out at 293 K with an Xcalibur diffractometer equipped with an area detector and graphite monochromated Mo Kα radiation (λ = 0.71073 Å). The data reduction was done with the CrysAlis RED program.[17] Information concerning data collection is summarized in Table 1. The structures were solved by direct methods using the SIR97 program.[18] Full matrix least-squares refinements were performed on F^2 using SHELXL97.[19] All non-hydrogen atoms were refined anisotropically. The hydrogen atoms of the pyrimidine ring were positioned geometrically and allowed to ride on their parent atoms with Uiso = 1.2Uiso(parent). The water hydrogen atoms were located in a Fourier difference map and introduced as fixed contributers with Uiso = 1.5Uiso(parent). All calculations were performed using the WinGX crystallographic software package.[20]

Results and Discussion

Structural Description

A structural feature common to compounds **1**, **2** and **5**, and encountered even in the previously characterized $\{[M(\mu\text{-pmdc})(H_2O)_2]\cdot H_2O\}_n$ materials (M = Fe, Co, Ni, Cu, Zn)[14], is the tetradentate μ-(κO,κN:κO",κN') coordination mode of the pyrimidine-4,6-dicarboxylate anion. Notably, species **3** constitutes an exception, in that the pmdc moiety adopts a pentadentate μ_3-(κO,κN:κO",κN':κO) coordination type. Despite the almost exclusive recurrence of one ligand coordination mode, the great coordination flexibility of manganese(II), tuned by means of temperature-directed entropic and

solvent effects, resulted in the isolation of different architectures based on the same [M(pmdc)] building block. Thus, as later described, the crystal structures of compounds **1**, **2** and **5** consist of $\{[M(\mu\text{-pmdc})]\}_n$ corrugated chains, in which the additional M(II) coordination sites are occupied by water molecules. At variance, the skeleton of the more compact species **3** can be rationalized as the fusion of corrugated parallel chains through already bound carboxylate oxygen atoms, replacing two of the coordinated water molecules of **1**, **2** and **5**.

Structural details and selected bond lengths for compounds **1**–**3** and **5** are gathered in Tables 1 and 2, respectively.

Insert TABLE 1 and TABLE 2 near here

$\{[Mn(\mu\text{-pmdc})(H_2O)_3]\cdot 2H_2O\}_n$ (1), $\{[Mn_2(\mu\text{-pmdc})_2(H_2O)_5]\cdot 2H_2O\}_n$ (2) and $\{[FeMn(\mu\text{-pmdc})_2(H_2O)_5]\cdot 2H_2O\}_n$ (5). Compound **1** crystallizes in the monoclinic $P2_1/c$ space group, while the isomorphous species **2** and **5** are triclinic, *P–1*. As anticipated, the three compounds contain 1D zig-zag polymeric chains built upon consecutive [M(pmdc)] monomers (M = Mn, Fe). The coordination about the metal centers, together with the labeling scheme, and a fragment of the polymeric chain are shown in Figure 1. The pmdc ligands adopt a μ-(κO,κN:κO",κN') coordination fashion, their *N*,*O*-chelation implying the formation, about each metal ion, of two five-membered rings. The remaining M(II) coordination sites are occupied by water molecules. In spite of this, some structural differences exist, which can be mainly traced back to *i*) the number of coordinated water molecules (3 in **1**; alternatively 2 and 3 in **2** and **5**), and *ii*) the metal content (Mn in **1** and **2**; mixed Fe:Mn = 1:1 in **5**). Indeed, in **1**, the unique crystallographically independent Mn(II) ion is bound to three water molecules in a *mer*-$[Mn(H_2O)_3]^{2+}$ fashion; the further assistance of two nitrogen and two oxygen atoms from two pmdc ligands implies an overall coordination sphere of the MnN_2O_5 kind, resembling a monocapped octahedron, with a bond significantly longer than the other ones (Table 2). On the contrary, in **2** and **5**, *cis*-$[M(H_2O)_2]^{2+}$ (M = Mn in **2**, Fe in **5**) and *mer*-$[Mn(H_2O)_3]^{2+}$ units alternate along the $\{[M(\mu\text{-pmdc})]\}_n$ chains.

Insert FIGURE 1 near here

Within the *cis*-$[M(H_2O)_2]^{2+}$ units, the M(II) ions show an octahedral MN_2O_4 stereochemistry, completed by the O and N atoms of two crystallographically independent ligands (pmdc1 and pmdc2 in the following). As in compound **1**, also in the *mer*-$[Mn(H_2O)_3]^{2+}$ units of **2** the Mn(II) centres display a monocapped octahedral MN_2O_5 stereochemistry, with one coordination distance slightly longer than the others (Table 2). Notably, in the heteronuclear compound **5**, the Fe(II) and Mn(II) metal centers are not statistically distributed along the 1D chains, yet they alternate in an ordered manner. Thus, the Mn(II) ions are exclusively hepta-coordinated, with virtually the same metal to ligand distances and angles as **2**. The Fe(II) ions adopt the octahedral environment, but with slightly shorter metal to ligand distances (*ca.* 0.05 Å) than in **2**, which agrees with its smaller ionic radii [$rFe(II)_{HS}$ = 0.75 *vs* $rMn(II)_{HS}$ = 0.81 Å, for coordination number 6].[21] Notably, the different preference we found for heptahedral coordination environments of the iron and manganese divalent cations is supported by a search throughout the CSD database [heptacoordinated metal complexes retrieved from the CSD database: 61(Mn^{2+}) *vs* 18(Fe^{2+})].[22]

As expected, the differently crowded metal centres induce *i*) significantly longer bond lengths around the hepta-coordinated ions [mean Mn–N = 2.428 Å (**1**) and 2.419 Å (**2**); mean Mn–O = 2.232 Å (**1**) and 2.225 Å (**2**)] than around the hexa-coordinated ones [mean M–N = 2.318 Å (**2**); mean M–O = 2.144 Å (**2**)]; *ii*) a more acute M···M···M angle in compound **1** (63.2º) than in **2** and **5** (71.2º in **2**); *iii*) a wider *N*,*O*-bite angle for the hexa-coordinated Mn(II) ions than for the hepta-coordinated ones (*e.g.* in **2** average values of 73.4° vs 69.9º are found, respectively), and *iv*) a significantly wider dihedral angle between the mean planes of the two ligands insisting on the same metal centre in **2** and **5** (74.14º in **2**) than in **1** (58.18º).

The bridged M···M distances are 6.767(1) Å in compound **1**, while 6.765(1) Å or 6.575(1) Å in compound **2**, and 6.705(1) Å or 6.521(1) Å in compound **5**, for pmdc1 and pmdc2, respectively.

In compound **1**, the pmdc ligand is essentially planar, with the carboxylate groups slightly turned off by (*ca.* 5.9º); somewhat larger values appear instead in **2**, with dihedral angles (for pmdc2) up to 16.2°.

In compound **1**, the chains run along the crystallographic ***b*** axis in a way that each one interacts with other four surrounding ones by means of an intricate hydrogen-bonding network (see Supp. Mat.). All together, H-bond interactions are present between the (coordinated and lattice) water molecules and the swinging oxygen atoms of the carboxylate groups (Figure 2a). Notably, one of the crystallization water molecules (O4w) is located in the void generated among four interconnected chains, while the second one (O5w) is deeply buried in the chains folds.

In compound **2** and **5**, the chains run along the crystallographic ***a*** axis (Figure 2b), their reciprocal disposition showing a great resemblance with that of **1**. Nonetheless, the smaller number of water molecules *per* metal ion allows a closer packing, in which every chain is directly hydrogen-bonded to six surrounding ones. The crystallization water molecules (O6w and O7w) are exclusively located within the folds of the chains, and they establish hydrogen-bond interactions with the host chain and a neighboring one.

Insert FIGURE 2 near here

{[Mn(μ$_3$-pmdc)(H$_2$O)]·H$_2$O}$_n$ (3). The single-crystal X-ray analysis showed that compound **3** crystallizes in the orthorhombic *Pbca* space group and consists of 2D layers of {[Mn(μ$_3$-pmdc)(H$_2$O)]}$_n$ formulation surrounded by crystallization water molecules. The Mn(II) ions show a distorted octahedral stereochemistry (Figure 3) of the MnN$_2$O$_4$ kind, completed by two pyrimidine nitrogen atoms and three carboxylate oxygen atoms from three symmetry related pmdc ligands, and by the oxygen atom of one water molecule. Thus, at variance with what found in compounds **1** and **2**, in **3** each pmdc ligand globally bridges three Mn(II) ions, adopting a pentadentate μ$_3$-(κO,κN:κO",κN':κO) coordination mode. *N*,*O*-chelation implies the formation, about each Mn(II) ion, of two five-membered rings (bite angles: 74.85 and 72.52º, respectively). The shortest M···M

distances within the two-dimensional coordination network are 3.487 Å along the bis-(μ-oxo) bridge and 6.664 Å through the μ-pyrimidine bridge. The pmdc ligand deviates slightly from the planarity, showing dihedral angles between the pyrimidine ring and the carboxylate groups of 3.3 and 9.4º.

Insert FIGURE 3 near here

The coordination network can be viewed as the fusion of polymeric 1D $\{[Mn(\mu\text{-pmdc})(H_2O)]\}_n$ zig-zag chains through a Mn–O bond from the already coordinated oxygen atom (O71) of a pmdc ligand belonging to an adjacent chain, which replaces the coordinated water molecules released on passing from **1** (or **2**) to **3**. Therefore, the dimensionality of the coordination connectivity is increased to yield an overall 2D folded skeleton showing oblong cavities (Figure 4) of *ca.* 3.6 × 6.8 Å (estimated after subtraction of the pertinent van der Waals radii), large enough to host two, symmetry related, O1w water molecules. These molecules interact, through hydrogen bonds, with the coordinated water molecule and the swinging oxygen atom of a neighbouring carboxylate group, connecting consecutive layers and creating a 3D network. Due to the symmetry requirements of the crystallographic *a* glide-plane, isolated cavities, and not channels, are formed (Figure 5), thus preventing the easy water molecules release and the adsorption of guest molecules. Accordingly, TG measurements indicated water loss only above 170 ºC (see Supp. Mat.).

Insert FIGURE 4 and FIGURE 5 near here

Mutual interconversion of 1, 2 and 3.

At this point, it is worth to emphasize some remarkable aspects on the synthesis of these compounds. The first one arises from the effect of the synthetic conditions, specially temperature and pressure, on the resulting crystal structure. Increasing the temperature leads to a smaller number of water molecules retained in the lattice, and, therefore, to an increase of the system entropy (thanks to the higher conformational freedom of the released water molecules). One consequence correlated to

the water release is the more effective packing of the resulting structure, as witnessed by the increase of the density values on going from **1** to **3** [1.895 (**1**), 1.920 (**2**) and 1.976 g cm^{-3} (**3**)], and the self-assembling of the 1D polymeric chains to yield an overall 2D covalent framework (**3**) under soft hydrothermal conditions. Indeed, it is well known that hydrothermal synthesis is an effective and powerful tool in the construction of high-dimensionality metal organic frameworks.[23] In these synthetic conditions, the metastable kinetic phases are more probably isolated rather than the thermodynamic ones;[24] therefore, when compound **3** is suspended in an aqueous solution and stirred for 48 hours at ambient conditions, the interconversion to the thermodynamically stable compound **1** is obtained.

The easy interconversion of compounds **1-3** is also worthy to be mentioned. All of them can be obtained from any of the other two by subjecting an aqueous suspension of the crushed starting material to the synthetic conditions detailed in Scheme 1. The presence of well shaped crystals in the resulting product in all cases possibly indicates that the interconversion process takes places through solubilization/crystallization process. Moreover, as confirmed by thermodiffractometric studies (Figure 6), the crystal structure similarities between compounds **1** and **2** allows the solid state transformation of **1** into **2** at 40 ºC, with retention of crystallinity, which is a nice example of an investigated topic in the recent literature.[25] At temperatures above 70 ºC, a further dehydration process leads to a poorly crystalline phase whose diffractogram does not bear any resemblance with those of the reported compounds. On the contrary, compound **4** is not involved in this kind of transformations. Upon release of water molecules, it does not change its structure, and reversibly adsorbs moisture, after heating, from the environment. On the other hand, the samples of compound **2** in room conditions slowly evolve to compound **1**, but compounds **3** and **4** are more stable in air with no evidence of crystal decomposition.

Insert FIGURE 6 near here

Comments on the crystal structure of compound 4

Species **4** possesses a clear stoichiometry, derived from thermogravimetric and elemental analyses. Its XRPD pattern (Figure 7) shows that it is a very crystalline material and can be described by a bcc lattice (a = 18.67 Å and V = 6507.8 $Å^3$, from a Le Bail refinement with pertinent figures of merit: Rwp = 0.084, Rp = 0.060). No extinctions other than $h+k+l = 2n+1$ could be observed, this indicating that many space groups are equally good candidates. Density considerations [D_{obs} = 1.65(2) g cm^{-3}, measured by flotation of a pressed disc of the powdered compound] lead to an estimated Z of 24 [D_{calc} = 1.68 g cm^{-3}]. Yet, no structural model could be built, neither using conventional reciprocal space techniques, nor employing simulated annealing direct space methods. While the former are known to fail for a low symmetry Laue class (indicating 'exact' overlap of non equivalent reflections), direct space solution failure is more surprising, but understandable: indeed, conventional intensity extraction methods use equipatitioning of overlapping reflections. Apparently, in non holoedric Laue groups, this problem has not yet found appropiate solution.[26] We have used different sample size and preparation modes, and repeatedly checked the reproducibility of the XRPD acquisitions, thus confirming the absence of preferred orientation or hydration/dehydration effects, yet without succeeding in solving the structure. However, during the reviewing process, it appeared in the literature[27] a sodalitic species of $[In(C_6N_2O_4H_2)_2Na_{0.36}K_{1.28}](NO_3)_{0.64}(H_2O)_{2.1}$ formula possessing a unit cell and crystallographic symmetry closely related to those of **4**. A preliminary structure solution has been carried out, based on structural information of the In(III) compound, and confirms that also **4** is a sodalitic porous material, containing large cavities (hydrated in air at room temperature), as found for the $M(X\text{-pymo})_2$ species (M = Cu, Pd; X-pymo = 5-X-pyrimidin-2-olate, X = H, F).[12a,12c,13]

Insert FIGURE 7 near here

Electronic and Magnetic Properties

The electronic spectra for compounds **1**–**4** do not show, as expected, any crystal field d-d transition but only intraligand π-π transitions centered at 38500 cm^{-1}. By contrast, the incorporation of Fe(II) ions in **5** gives rise to the apparition of strong band at 18900 cm^{-1} which is attributed to a possible intervalence transition between Fe and Mn and a d-d absorption band centered at 9700 cm^{-1} typical of high spin Fe(II).[28]

Compounds **1**–**3** show a room temperature $\chi_M T$ value (Table 3) close to that expected for an uncoupled manganese(II) ion (g = 2.0, $\chi_M T$ = 4.38 cm^3 K mol^{-1}). In the case of **5** the value falls in the range between those expected for manganese(II) and high spin iron(II). In all cases, upon cooling the sample the $\chi_M T$ value decreases gradually, indicating an overall antiferromagnetic behaviour (Figure 8). In addition, the absence of any maximum in the χ_M curve suggests the occurrence of weak magnetic interactions. This behaviour agrees with the reported antiferromagnetic interactions for metal ions containing e_g unpaired electrons bridged by pyrimidine type ligands,[13,29] in contrast with the ferromagnetic behaviour usually observed for compounds containing only t_{2g} unpaired electrons.[30]

Insert FIGURE 8 and TABLE 3 near here

Taking into account the molecular structures of compounds **1** and **2**, their magnetic data have been fitted using the classical spin Heisenberg model for a regular antiferromagnetic chain with S = 5/2 ($H = -J\sum S_i S_{i+1}$).[31] It deserves to note that the magnetic interactions between the paramagnetic centers in these complexes take place mainly through the pyrimidine ring since, for a bis-bidentate pmdc bridge, the contribution of the carboxylato groups can be considered negligible due to the long magnetic pathway involving these groups.[14,32] In fact, the obtained *J* values for compounds **1** and **2** agree fairly well with the previously reported magnetic data for pyirimidine bridged Mn(II) complexes (*J* ranging from –0.2 to –0.3 cm^{-1}).[29a,33]

The regular alternance of high spin Fe^{2+} (d^6) and Mn^{2+} (d^5) ions along the chains of compound **5** could lead to a ferrimagnetic behaviour at low temperatures if the magnetic interaction through the pmdc bridges were strong enough. In the present case, the typical minimum on the $\chi_M T$ curve of a

ferrimagnetic compound is not observed. This fact has been attributed to the weakness of the magnetic interactions; indeed, the $\chi_M T$ value at 2 K is 1.33 cm^3 K mol^{-1}, far above the theoretical value of 0.87 cm^3 K mol^{-1} for 0.5 unpaired electrons per metal center. In order to estimate the value of the magnetic coupling in compound **5**, its magnetic data have been fitted to the analytical expression derived by Drillon et al. for alternating chains of classical spins,[34] giving a value of –0.38 cm^{-1}.

The complex connectivity among the metal centers in compound **3** and the preliminary results on the crystal structure of compound **4** preclude the quantitative estimation of the coupling constant. Therefore, in order to make a comparative study on the efficiency of the pmdc bridges in transmitting the magnetic interaction, the susceptibility data have been satisfactorily fit to the Curie-Weiss equation $\chi_M = C/(T-\theta)$, [$C = Ng^2\mu^2S(S+1)/3k$]. The fitted values (Table 3) agree with a weak antiferromagnetic coupling of the metal centres transmitted through the pmdc bridges and indicates a slightly stronger interaction for compound **3** compared with compounds **1** and **2** (as witnessed by the θ values), in good agreement with the higher connectivity among the metal centers. The results show a weaker interaction than those found for the Fe-Cu series,[14] which should be related to the increasing number of t_{2g}-t_{2g} and t_{2g}-e_g ferromagnetic terms along the series.

Adsorption properties

The gas adsorption performances of solids **1**, **2**, **3** and **4** towards N_2 and CO_2 have been studied in order to determine their textural properties and their potential use for gas separation and storage purposes. The results show that whereas **1**–**3** do not adsorb the tested gases, **4** behaves as a microporous material.

The adsorption isotherm of **4** towards N_2 (Figure 9a) possesses a type I–IV hybrid shape, with a (type H1) hysteresis loop at relative pressures above 0.8, which can be attributed to textural mesoporosity arising from interparticle mesopores. The isotherm also exhibits a sharp knee at low relative pressures ($p/p^0 < 0.01$) followed by a plateau (corresponding to the filling of the microporous structure), indicating that the permanent porosity of the sample is mainly composed of micropores, of

rather uniform size consistent with the preliminary crystallographic data (see above). The low onset pressure and the sharp rise of the isotherm indicate that a deep potential well forms in the micropores. Fitting the isotherm to the Langmuir equation in the low pressure region ($p/p^0 < 0.2$) gives a considerably high surface area value of 410 m^2g^{-1}.

Insert FIGURE 9 near here

Even the CO_2 adsorption measurements indicate that **4** possesses permanent porosity in the microporous region, which is manifested by the steep slope of the type I isotherm in the low p/p^0 relative pressure region (see Figure 9b). The amount of CO_2 sorbed at 293 K and 650 torr is considerably high, namely 40 cm^3g^{-1}. This high storage capacity at room temperature should be indicative of the full accessibility of the adsorbate molecules to the porous network and that, as previously mentioned, a deep potential well forms in the pores. The adsorption performance of **4** toward CO_2 clearly approaches the values found for the best porous pyridimine derivatives, being surpassed only by the $[Pd(X\text{-pyrimidine-2-olate})_2]_n$ (X = H, F)[13] sodalitic frameworks, and should be taken as a further proof of the efficiency of the pyrimidine based ligands in the formation of highly accessible porous networks. In this regard, the dianionic nature of the pmdc ligand results in a higher metal ion to organic ligand ratio compared to the previously reported $[M(\text{pyrimidinolate})_2]_n$ materials.[13,35] The presence of a higher number of metal ions in the network may result in a higher accessibility to the polarising metal centers with its consequent high adsorbate-adsorbent interaction.[36]

Conclusions

The anionic nature of the pmdc ligand leads to the formation of neutral and, in the case of **4**, thermally robust, networks. The variation of the synthetic conditions coupled to the plasticity of Mn(II) leads to a wide diversity of structural, magnetic and adsorptive properties, with examples of 1D, 2D and even (microporous) 3D species. The crystal to crystal interconversion pathways among these species, favoured by temperature and humidity changes, has been studied by means of a

combination of conventional single-crystal techniques and powder diffraction methods. Work can be anticipated in studying the sorptive properties of **4** toward environmentally relevant gases other than N_2 and CO_2, and in extending this kind of reactions to other transition metals ions.

Acknowledgements. This work was supported by the Spanish Ministerio de Educación y Ciencia (MAT2005–03047, CTQ2005-00329/BQU, SB-2005-0115, HI2006-0116, and by the Italian Ministero dell'Università e della Ricerca (PRIN 2006: "Materiali ibridi metallo-organici multifunzionali con leganti poliazotati"). The finantial support by Fondazione Cariplo is also acknowledged. G.B. thanks the Eusko Jaurlaritza/Gobierno Vasco for a doctoral fellowship (BF102.79). W.G.W. thanks the Spanish Ministerio de Educación y Ciencia for a postdoctoral fellowship. G.T. thanks the Italian Ministero dell'Università e della Ricerca for a doctoral grant (Progetto Giovani 2006). The authors are also grateful to to Prof. N. Masciocchi and Prof. M. A. Romero for helpful discussions.

Supporting Information Available: Hydrogen bonding parameters. Thermogravimetric curves (TG/DTA) of compounds **1**–**4**. X-ray crystallographic files in CIF format. This material is available free of charge via the Internet at http://pubs.acs.org.

TABLE CAPTIONS

Table 1. Single-Crystal Data and Structure Refinement Details for Compounds **1**–**3** and **5**.

Table 2. Selected Bond Lengths (Å) in Compounds **1**–**3** and **5**.

Table 3. Best-Fit Values for compounds **1**–**5**.

FIGURE CAPTIONS

Scheme 1. Routes and synthetic conditions for the interconversion among compounds **1**, **2**, **3** and **4**.

Figure 1. Perspective drawing of a fragment of the one-dimensional chain for compounds **1** (a) and **2**/**5** (b). The inner boxes show Ortep graphics of the M(II) coordination environments.

Figure 2. Left: view of the crystal packing of (a) compound **1** along the [010] direction, and (b) compound **2** along [100]. Right: crystallization water molecules inserted in the folds of the 1D chains in both compounds. Colour code: carbon (grey), nitrogen (green), oxygen atoms of carboxylate groups and coordinated water molecules (blue), and crystallization water molecules (pink). Hydrogen atoms were omitted for clarity.

Figure 3. ORTEP view of the M(II) coordination environment of compound **3**, showing the numbering scheme.

Figure 4. View of the 2D skeleton of compound **3** (left), showing the μ-oxo bridges (in red) among the chains (right).

Figure 5. (a) View of compound **3** along the [100] direction and (b) schematic view of the sheets stacking along the [001] direction. Upper and lower sheets are represented in different colours.

Figure 6. Selected XRPD patterns of the thermal treatment of compound **1**.

Figure 7. Le Bail refinement of species **4** in terms of experimental (blue), calculated (red) and difference (grey) profiles. The peak markers are shown at the bottom. Horizontal axis: 2θ, deg; vertical axis: counts.

Figure 8. Thermal behaviour of the $\chi_M T$ values at 5 kOe for compounds **1**-**5**. The values haves been calculated *per* Mn except for **5**, for which they have been expressed for a $Mn_{0.5}Fe_{0.5}$ content. (a) circles, **1**; squares, **2**; diamonds, **5**. (b) circles, **3**; squares, **4**.

Figure 9. (a) N_2 adsorption isotherm at 77 K for **4**. (b) CO_2 adsorption isotherm at 293 K for **4**. Open symbols denote desorption.

TABLE 1

	1	**2**	**5**	**3**
Empirical formula	$C_6H_{12}MnN_2O_9$	$C_{12}H_{18}Mn_2N_4O_{15}$	$C_{12}H_{18}MnFeN_4O_{15}$	$C_6H_6MnN_2O_6$
Formula weight	311.12	568.18	569.09	257.07
Crystal system	Monoclinic	Triclinic	Triclinic	Orthorhombic
Space group	*P2₁/c*	*P-1*	*P-1*	*Pbca*
a (Å)	12.204(5)	7.767(1)	7.7854(6)	9.971(1)
b (Å)	7.093(5)	10.281(2)	10.2442(8)	12.534(2)
c (Å)	14.846(4)	13.451(2)	13.395(1)	13.830(1)
α (°)	90	100.18(1)	100.388(1)	90
β (°)	121.96(2)	103.52(1)	103.293(1)	90
γ (°)	90	103.82(1)	103.764(1)	90
V (Å^3)	1090.3(10)	982.9(3)	978.2(1)	1728.4(3)
Z	4	2	2	8
D_{obs} (g cm^{-3})	1.89(1)	1.91(1)	1.93(1)	1.97(1)
D_{calc} (g cm^{-3})	1.895	1.920	1.932	1.976
μ (mm^{-1})	1.258	1.375	1.477	1.540
R1 [a]	0.0598	0.0412	0.0358	0.0321
wR2 [b]	0.1355	0.0720	0.0897	0.0780

[a] $R1 = \Sigma\,(||F_o| - |F_c||) / \Sigma\,|F_o|$. [b] $wR2 = [\Sigma w(||F_o| - |F_c||)^2 / \Sigma w|F_o|^2]^{1/2}$

TABLE 2

1		2		5		3	
Mn1–N1	2.351(2)	Mn1–N11	2.337(2)	Fe1–N11	2.269(2)	Mn1–N1	2.323(2)
Mn1–O81	2.196(2)	Mn1–N21	2.288(2)	Fe1–N21	2.228(2)	Mn1–O81	2.093(1)
Mn1–N3a	2.506(2)	Mn1–O2w	2.167(2)	Fe1–O2w	2.162(2)	Mn1–N3a	2.302(1)
Mn1–O71a	2.186(2)	Mn1–O1w	2.108(2)	Fe1–O1w	2.078(2)	Mn1–O71a	2.177(1)
Mn1–O1w	2.294(2)	Mn1–O181	2.129(2)	Fe1–O181	2.080(2)	Mn1–O71b	2.184(1)
Mn1–O2w	2.193(2)	Mn1–O281	2.160(2)	Fe1–O281	2.112(2)	Mn1–O1w	2.151(1)
Mn1–O3w	2.290(2)	Mn2–N13a	2.405(2)	Mn1–N13a	2.401(2)		
		Mn2–N23	2.433(2)	Mn1–N23	2.435(2)		
		Mn2–O171a	2.204(2)	Mn1–O171a	2.198(2)		
		Mn2–O271	2.203(1)	Mn1–O271	2.199(2)		
		Mn2–O3w	2.241(2)	Mn1–O3w	2.255(2)		
		Mn2–O4w	2.245(2)	Mn1–O4w	2.251(2)		
		Mn2–O5w	2.197(2)	Mn1–O5w	2.209(2)		

Symmetry codes: **1**: (a) –x, y – 1/2, –z – 3/2. **2** and **5**: (a) x+1, y, z. **3**: (a) 1/2 + x, 1/2 – y, 1 – z; (b) – 1/2 – x, – 1/2 + y, z.

TABLE 3

Compound	$\chi_M T$ (300 K)	J (cm^{-1})	g	C (cm^3 K mol^{-1})	θ (K)
1[a]	4.28	–0.18	2.00	4.30	–1.9
2[a]	4.38	–0.22	2.00	4.40	–1.7
3	4.51	---	---	4.53	–2.4
4	3.89	---	---	3.92	–1.5
5[b]	3.87	-0.38	2.00(Mn)/2.18(Fe)	3.92	–2.5

[a] 1D Heisenberg model; [b] 1D alternate classical spins.

SCHEME 1

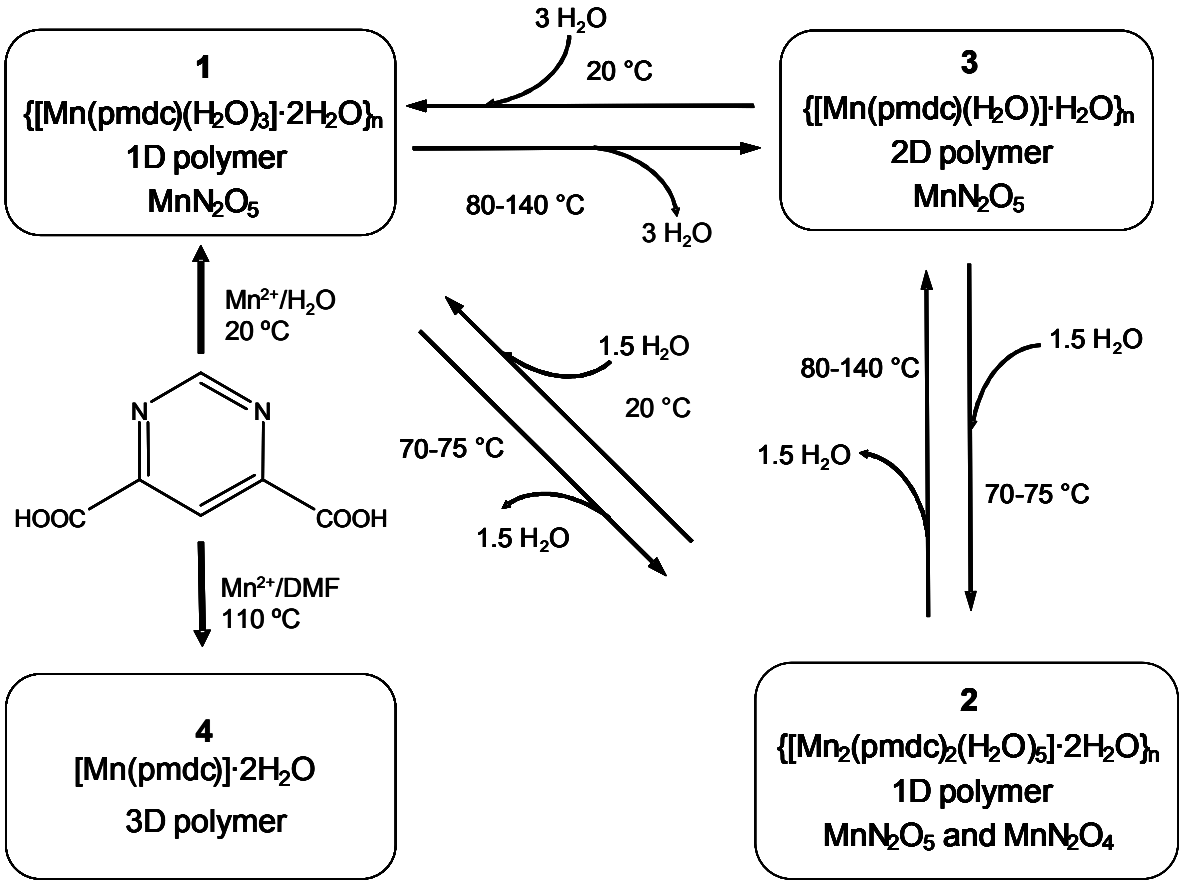
1
{[Mn(pmdc)(H2O)3]·2H2O}n
1D polymer
MnN2O5
3 H2O
20 °C
80-140 °C
3 H2O
3
{[Mn(pmdc)(H2O)]·H2O}n
2D polymer
MnN2O5
Mn2+/H2O
20 °C
N
N
HOOC
COOH
Mn2+/DMF
110 °C
1.5 H2O
20 °C
70-75 °C
1.5 H2O
80-140 °C
1.5 H2O
1.5 H2O
70-75 °C
4
[Mn(pmdc)]·2H2O
3D polymer
2
{[Mn2(pmdc)2(H2O)5]·2H2O}n
1D polymer
MnN2O5 and MnN2O4

FIGURE 1

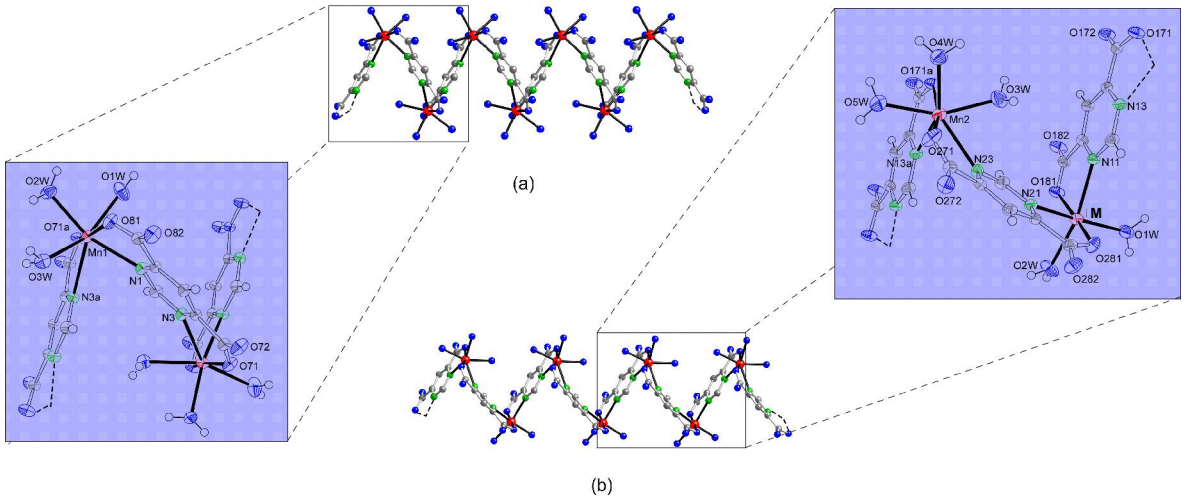
O2W
O1W
O71a
O81
O82
Mn1
O3W
N1
N3a
N3
O72
O71
(a)
O4W
O171a
O3W
O5W
Mn2
O271
N13a
N23
O272
O172
O171
N13
O182
N11
O181
N21
M
O1W
O2W
O281
O282
(b)

FIGURE 2

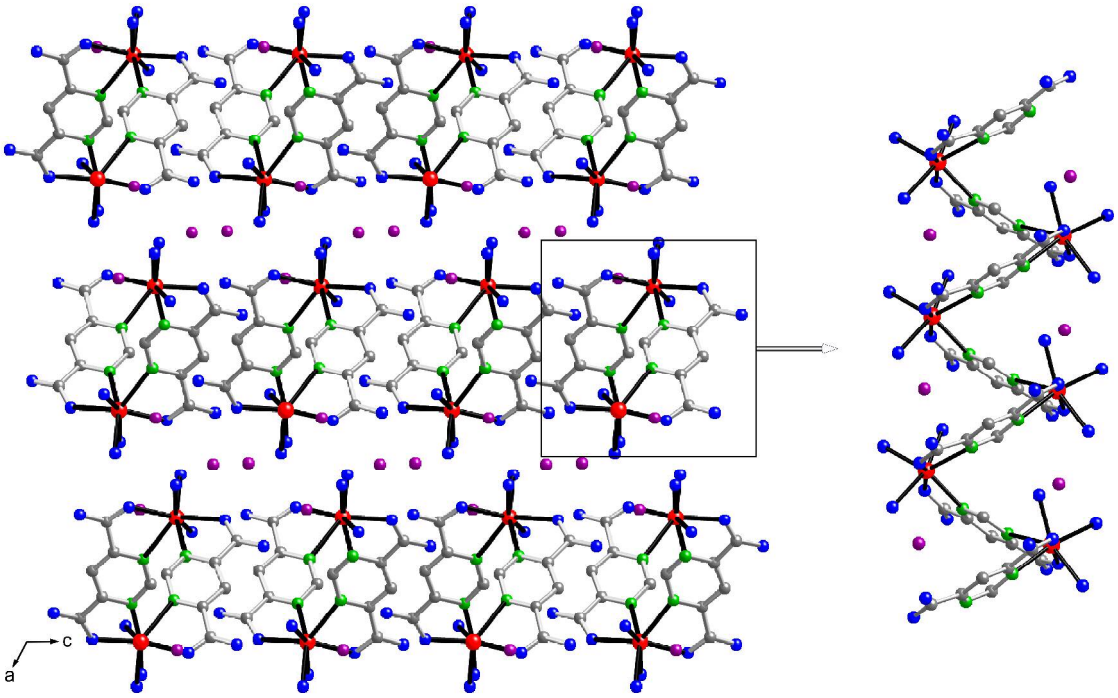

(a)

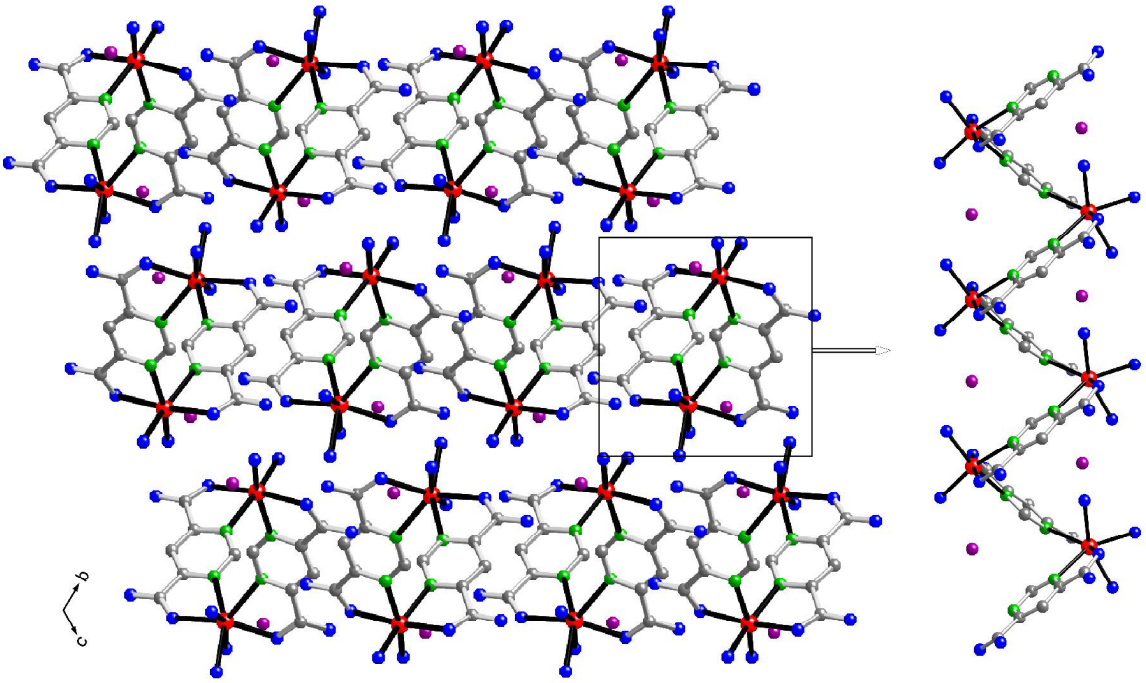

(b)

FIGURE 3

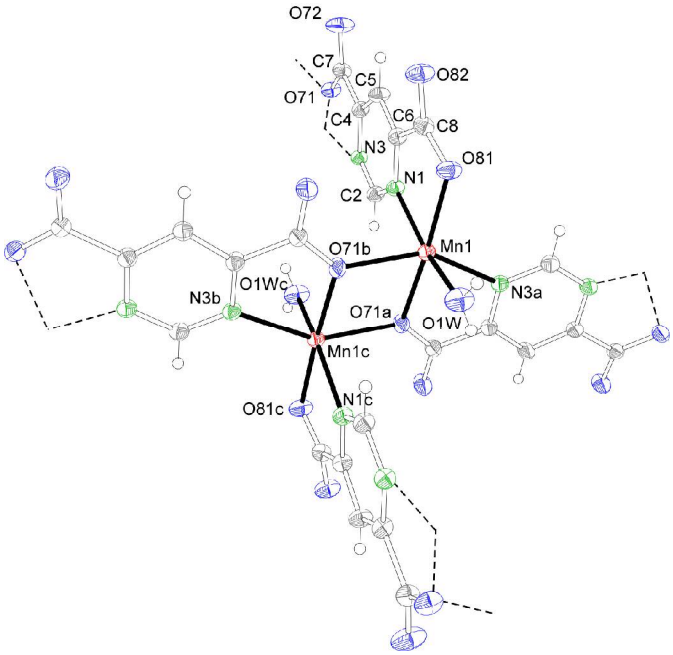

FIGURE 4

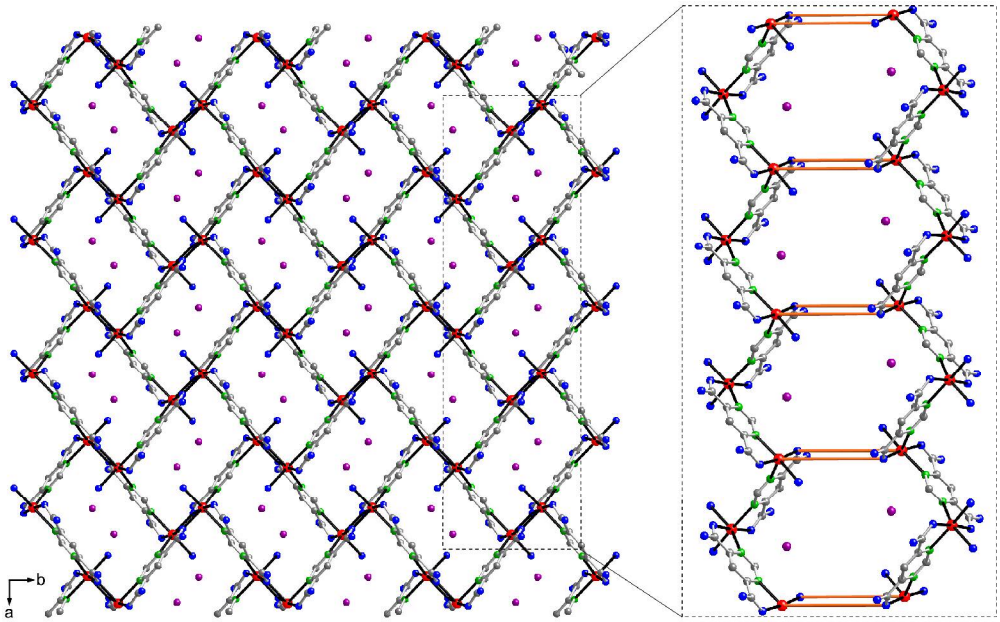

FIGURE 5

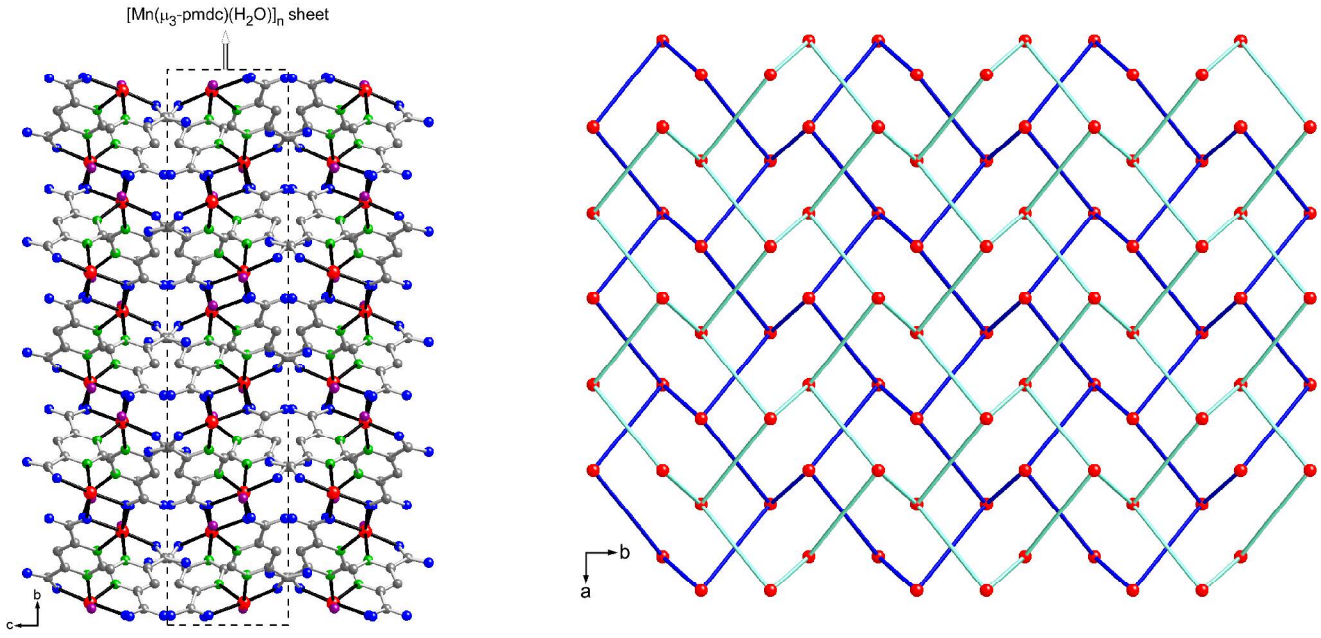

(a) (b)

FIGURE 6

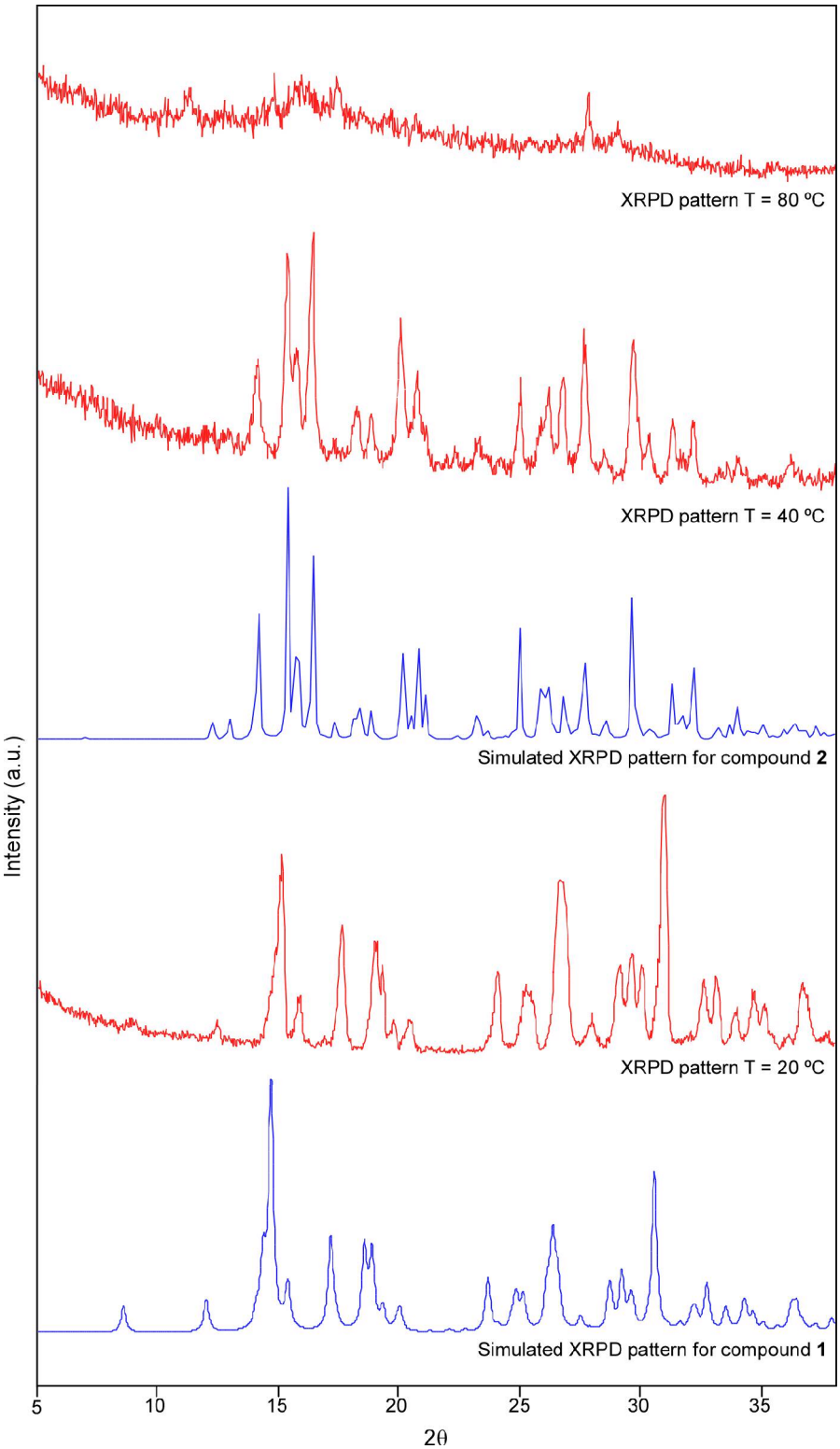
XRPD pattern T = 80 ºC
XRPD pattern T = 40 ºC
Simulated XRPD pattern for compound 2
XRPD pattern T = 20 ºC
Simulated XRPD pattern for compound 1
Intensity (a.u.)
5
10
15
20
25
30
35
2θ

FIGURE 7

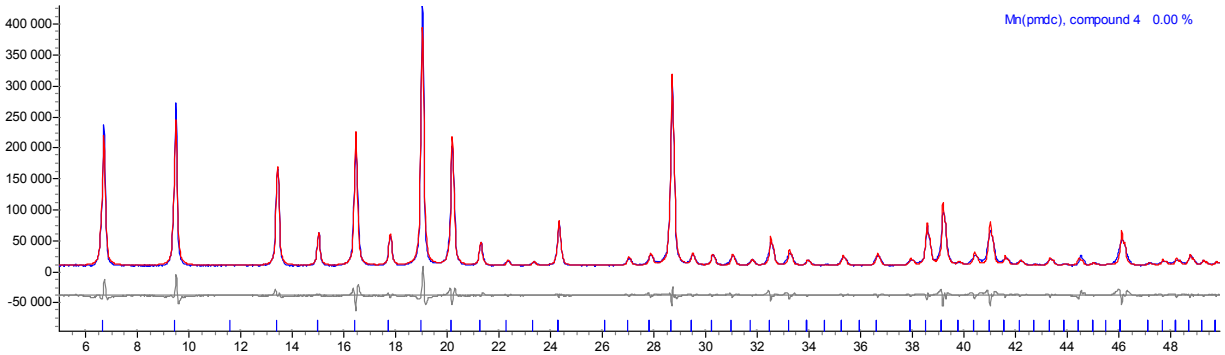
Mn(pmdc), compound 4 0.00 %
400 000
350 000
300 000
250 000
200 000
150 000
100 000
50 000
0
-50 000
6
8
10
12
14
16
18
20
22
24
26
28
30
32
34
36
38
40
42
44
46
48

FIGURE 8

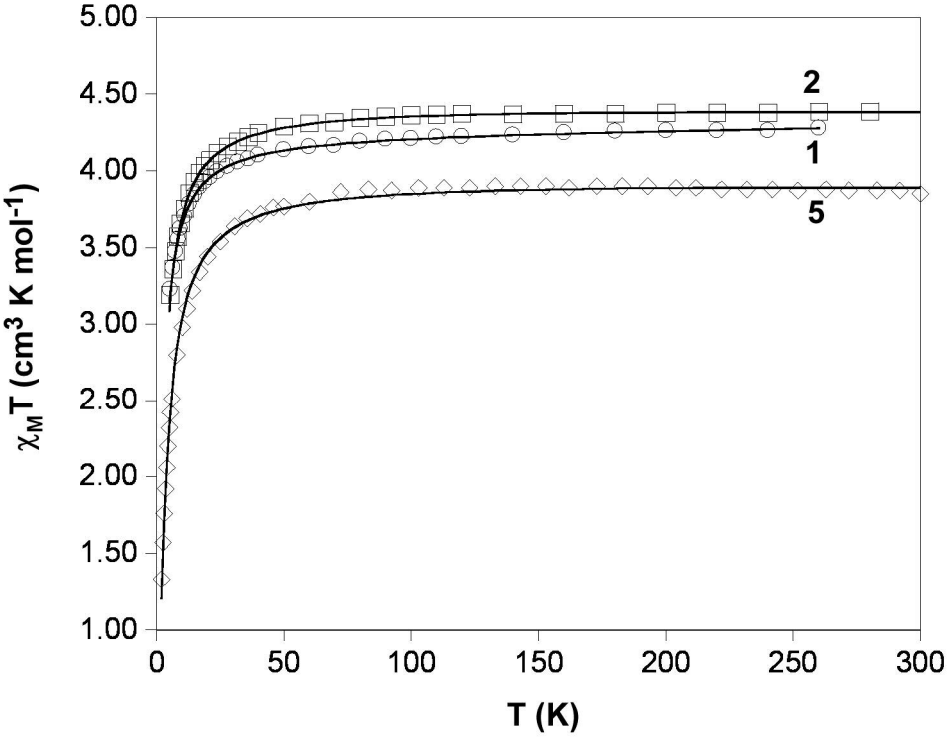
5.00
4.50
4.00
3.50
3.00
2.50
2.00
1.50
1.00
0
50
100
150
200
250
300
T (K)
$\chi_M T$ (cm^3 K mol^{-1})
2
1
5

(a)

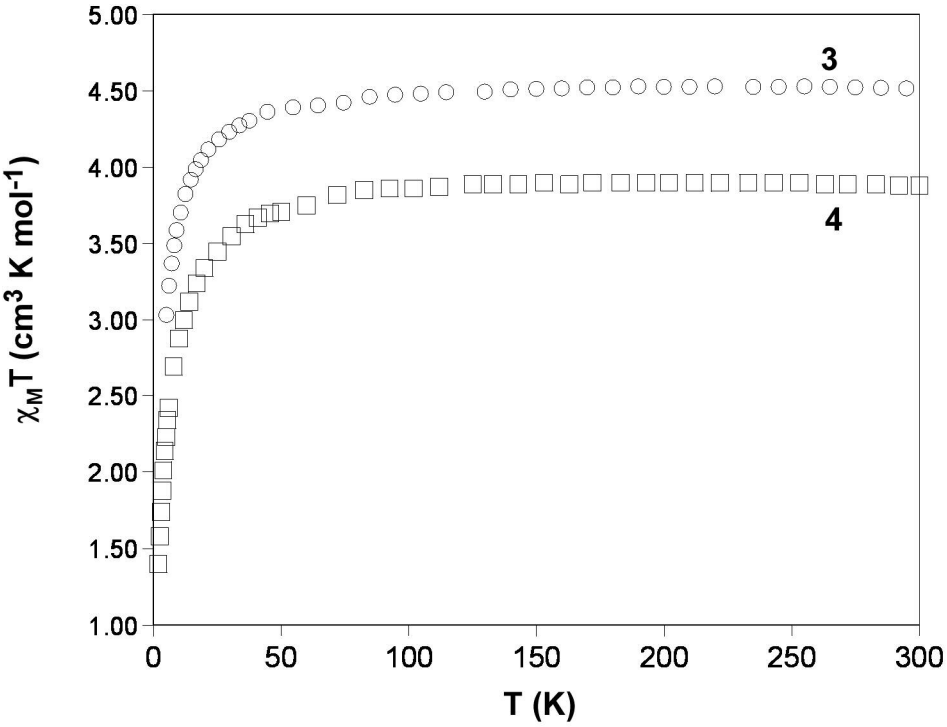
5.00
4.50
4.00
3.50
3.00
2.50
2.00
1.50
1.00
0
50
100
150
200
250
300
T (K)
$\chi_M T$ (cm^3 K mol^{-1})
3
4

(b)

FIGURE 9

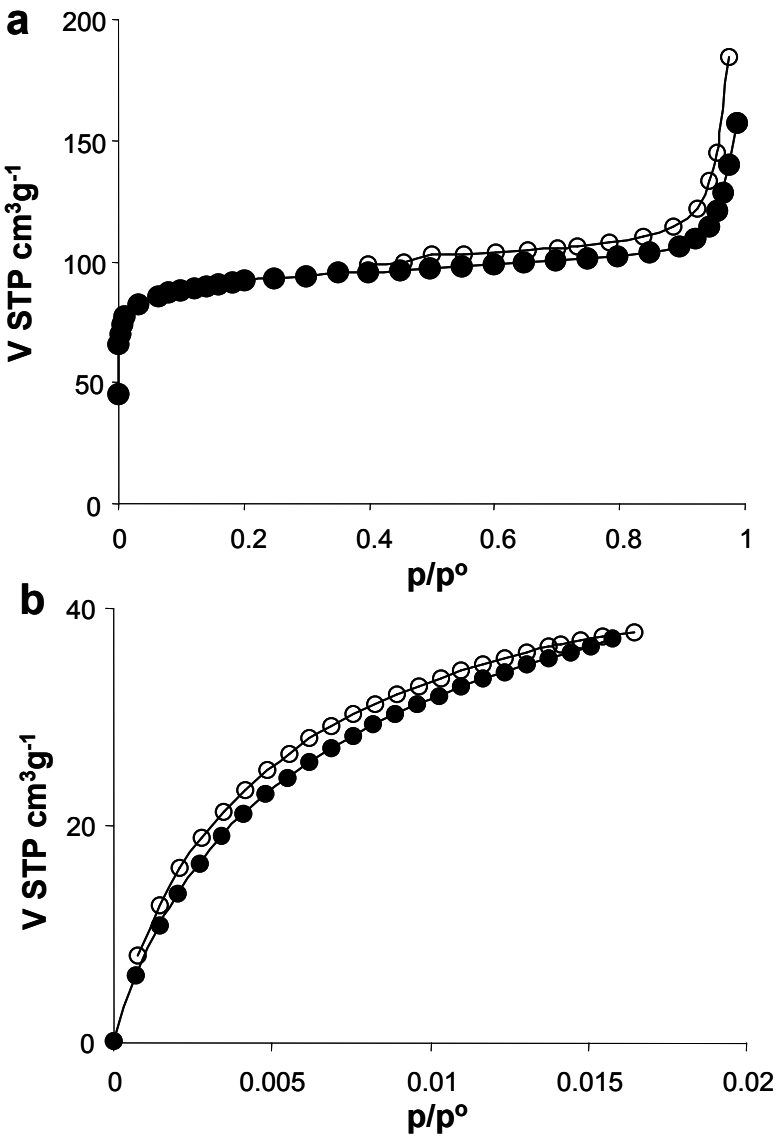
a
200
150
100
50
0
V STP cm3g-1
0
0.2
0.4
0.6
0.8
1
p/po
b
40
20
0
V STP cm3g-1
0
0.005
0.01
0.015
0.02
p/po

References

[1] (*a*) Kepert, C. J. *Chem. Commun*. **2006**, 695. (*b*) Posch, D.; Ruiz-Molina, D.; Veciana, J. *Chem. Soc. Rev*. **2007**, *36*, 770. (*c*) Janiak, C. *Dalton Trans.* **2003**, 2781. (*d*) Kitagawa, S.; Kitaura, R.; Noro, S. *Angew. Chem. Int. Ed.* **2004***, 43*, 2334. (*e*) Robin, A. Y.; Fromm, K. M. *Coord. Chem. Re*v. **2006**, *250*, 2127.

[2] Mueller, U.; Schubert, M.; Teich, F.; Puetter, H.; Schierle-Arndt, K.; Pastre, J. *J. Mater. Chem*. **2006**, *16*, 626.

[3] Matsuda, R.; Kitaura, R.; Kitagawa, S.; Kubota, Y.; Belosludov, R. V.; Kobayashi, T. C.; Sakamoto, H.; Chiba, T.; Takata, M.; Kawazoe, Y.; Mita, Y. *Nature* **2005**, *436*, 238.

[4] (*a*) Pan, L.; Olson, D. H.; Ciemnolonski, L. R.; Heddy, R.; Li, J. *Angew. Chem. Int. Ed.* **2006**, *45*, 616. (*b*) Hayashi, H.; Cote, A. P.; Furukawa, H.; O'Keeffe, M.; Yaghi, O. M. *Nature Mater.* **2007**, *6*, 501.

[5] Llabrés i Xamena, F. X.; Abad, A.; Corma, A.; García, H. *J. Cat.* **2007**, *250*, 294.

[6] Uemura, T.; Kitaura, R.; Ohta, Y.; Nagaoka, M.; Kitagawa, S. *Angew. Chem. Int. Ed.* **2006**, *45*, 4112.

[7] (*a*) Dybtsev, D. N.; Nuzhdin, A. L.; Chun, H.; Bryliakov, K. P.; Talsi, E. P.; Fedin, V. P.; Kim, K. *Angew. Chem*. *Int. Ed*. **2006**, *45*, 916. (*b*) Wu, C.-D.; Hu, A.; Zhang, L.; Lin, W. *J. Am. Chem. Soc*. **2005**, *127*, 8940.

[8] Xiao, B.; Wheatley, P. S.; Zhao, X.; Fletcher, A. J.; Fox, S.; Rossi, A. G.; Megson, I. L.; Bordoga, S.; Regli, L.; Thomas, K. M.; Morris, R. E. *J. Am. Chem. Soc.* **2007**, *129*, 1203.

[9] Galli, S.; Masciocchi, N.; Cariati, E.; Sironi, A.; Barea, E.; Haj, M. A.; Navarro, J. A. R.; Salas**,** J. M. *Chem. Mater*. **2005**, *17*, 4815.

[10] (*a*) Beobide, G.; Castillo, O.; Luque, A.; García-Couceiro, U.; García-Terán, J. P., Román, P. *Inorg. Chem*. **2006**, *45*, 5367. (*b*) Masciocchi, N.; Galli, S.; Sironi, A.; Galindo, M. A.; Barea, E.; Romero, M. A.; Salas, J. M.; Navarro, J. A. R., Santoyo, F. *Inorg. Chem*. **2006**, *45*, 7612. (*c*) Navarro, J. A. R.; Barea, E.; Salas, J. M.; Masciocchi, N.; Galli, S.; Sironi, A. *Inorg. Chem*. **2007**, *46*, 2988.

[11] Masciocchi, N.; Ardizzoia, G. A.; LaMonica, G.; Maspero, A.; Sironi, A. *Eur. J. Inorg. Chem.* **2000**, 2507.

[12] (*a*) Tabares, L. C.; Navarro, J. A. R.; Salas, J. M. *J. Am. Chem. Soc*. **2001**, *123*, 283. (*b*) Barea, E.; Navarro, J. A. R.; Salas, J. M.; Masciocchi, N.; Galli, S.; Sironi, A. *Polyhedron* **2003**, *22*, 3051. (*c*) Barea, E.; Navarro, J. A. R.; Salas, J. M.; Masciocchi, N.; Galli, S.; Sironi, A. *J. Am. Chem. Soc*. **2004**, *125*, 3015. (*d*) Barea, E.; Navarro, J. A. R.; Salas, J. M.; Quirós, M. *Dalton Trans*. **2005**, 1743.

[13] (*a*) Navarro, J. A. R.; Barea, E.; Salas, J. M.; Masciocchi, N.; Galli, S.; Sironi, A.; Ania, C. O.; Parra, J. B. *Inorg. Chem.* **2006**, *45*, 2397. (b) Navarro, J. A. R.; Barea, E.; Salas, J. M.; Masciocchi, N.; Galli,

S.; Sironi, A.; Ania, C. O.; Parra, J. B. *J. Mater. Chem.* **2007**, *17*, 1939. (c) Navarro, J. A. R.; Barea, E.; Salas, J. M.; Rodríguez-Diéguez, A.; Ania, C. O.; Parra, J. B.; Masciocchi, N.; Galli, S.; Sironi, A.; *J. Am. Chem. Soc.* **2008**, *129*, 3978.

[14] Beobide, G.; Castillo, O.; Luque, A.; García-Couceiro, U.; García-Terán, J. P.; Román, P. *Dalton Trans.* **2007**, 2669.

[15] Hunt, R. R.; McOmie, J. F. W.; Sayer, E. R. *J. Chem. Soc.* **1959**, 525-530.

[16] Earnshaw, A. *Introduction to Magnetochemistry*; Academic Press: London, **1968**.

[17] CrysAlis RED, version 1.170, Oxford Diffraction, Wroclaw, Poland, **2003**.

[18] Altomare, A.; Burla, M. C.; Camalli, M.; Cascarano, G. L.; Giacovazzo, C.; Guagliardi, A.; Moliterni, A. G. G.; Spagna, R. *J. Appl. Crystallogr.* **1999**, *32*, 115-119.

[19] Sheldrick, G. M. *SHELXS97 and SHELXL97*; University of Göttingen, Germany, **1997**.

[20] Farrugia, L. J. *WINGX. A Windows program for crystal structure analysis*; University of Glasgow, Great Britain, **1998**.

[21] Shannon, R. D. *Acta Crystallogr.* **1976**, ***A32***, 751.

[22] Allen, F. H. *Acta Crystallogr., Sect. B* **2002**, *58*, 380-388.

[23] Cheetham, A. K.; Rao, C. N. R.; Feller, R. K. *Chem. Commun.* **2006**, 4780.

[24] Hagrman, P. J.; Finn, R. C.; Zubieta, J. *Solid State Sci.* **2001**, *3*, 745.

[25] Habib, H. A.; Sanchiz, J.; Janiak, C. *Dalton Trans.* **2008**, 1734.

[26] Altomare, A. personal communication.

[27] Sava, D. F.; Kravtsov, V. Ch.; Nouar, F.; Wojtas, L. Eubank, J. F.; Eddaoudi, M. *J. Am. Chem. Soc.* **2008**, *130*, 3768.

[28] Garner, M.; Lewinski, K.; Pattek-Janczyk, A.; Reglinski, J.; Sieklucka, B.; Spicer, M. D.; Szaleniec, M. *Dalton Trans.* **2003**, 1181.

[29] (a) Ishida, T.; Kawakami, T.; Mitsubori, S.; Nogami, T.; Yamaguchiand, K. And Iwamura, H.; *J. Chem. Soc., Dalton Trans.* **2002**, 3177. (b) Ezhura, T.; Endo, K.; Matsuda, K.; Aoyama, Y. *New J. Chem.* **2000**, *24*, 609. (c) Manson, J. L.; Gu, J.; Schlueter J. A.; Wang, H. H. *Inorg. Chem.* **2003**, ***42***,

3950. (d) Yasui, M.; Ishikawa, Y.; Akiyama, N.; Ishida, T.; Nogami, T.; Iwasaki, F. *Acta Crystallogr., Sect. B* **2001**, ***57***, 288.

[30] (a) Ishida, T.; Mitsubori, S.; Nogami, T.; Takeda, N.; Ishikawa, M.; Iwamura, H. *Inorg. Chem.* **2001**, *40*, 7059. (b) Mohri, F.; Yoshizawa, K.; Yamabe, T.; Ishida, T.; Nogami, T. *Mol. Eng.* **1999**, ***8***, 357.

[31] Fisher, M. E. *Am. J. Phys.* **1964**, *32*, 343.

[32] Beobide, G.; Castillo, O.; García-Couceiro, U.; García-Terán, J. P.; Luque, A.; Martínez-Ripoll, M.; Román, P. *Eur. J. Inorg. Chem.* **2005**, 2586.

[33] (a) Lloret, F.; Julve, M.; Cano, J.; De Munno, G. *Mol. Cryst. Liq. Cryst.* **1999**, *334*, 569. (b) Escuer, A.; Vicente, R.; Mautner, F. A.; Goher, M. A. S.; Abu-Youssef, M. A. M.; *Chem. Commun.* **2002**, 64.

[34] Drillon, M.; Coronado, E.; Beltran, D; Georges, R. *Chem. Phys.* **1983**, *79*, 449.

[35] Navarro, J. A. R.; Barea, E.; Salas, J. M.; Romero, M. A.; Quirós, M.; Masciocchi, N.; Galli, S.; Sironi, A.; Lippert, B. *J. Solid State Chem*. **2005**, *178*, 2436.

[36] (a) B. Chen, N. W.;Ockwig, A. R.; Millward, D. S. Contreras, O. M. Yaghi, *Angew. Chem. Int. Ed*. **2005**, *44*, 4745. (b) Dinca, M.; Yu, A. F.; Long, J. R. *J. Am. Chem. Soc.* **2006**, *128*, 8904.